Chemistry–A European Journal
Research Article
doi.org/10.1002/chem.202302968
Chemistry Europe
European Chemical Societies Publishing
www.chemeurj.org

Special Collection

Selective Perchlorate Sensing Using Electrochemical Impedance Spectroscopy with Self-Assembled Monolayers of *semiaza*-Bambusurils

Raman Khurana,[a] Fuad Alami,[d] Christian A. Nijhuis,[d] Ehud Keinan,*[c] Jurriaan Huskens,*[b] and Ofer Reany*[a]

In the last two decades, perchlorate salts have been identified as environmental pollutants and recognized as potential substances affecting human health. We describe self-assembled monolayers (SAMs) of novel *semiaza*-bambus[6]urils (*semiaza*-BUs) equipped with thioethers or disulfide (dithiolane) functionalities as surface-anchoring groups on gold electrodes. Cyclic voltammetry (CV) with $Fe(CN)_6^{3-/4-}$ as a redox probe, together with X-ray photoelectron spectroscopy (XPS), atomic force microscopy (AFM) and ellipsometry, were employed to characterize the interactions at the interface between the anchoring groups and the metal substrate. Data showed that the anion receptors' packing on the gold strongly depends on the anchoring group. As a result, SAMs of BUs with lipoic amide side chains show a concentration-dependent layer thickness. The BU SAMs are extremely stable on repeated electrochemical potential scans and can selectively recognize perchlorate anions. Our electrochemical impedance spectroscopy (EIS) studies indicated that semiaza-BU equipped with the lipoic amide side chains binds perchlorate (2–100 mM) preferentially over other anions such as F^-, Cl^-, I^-, AcO^-, $H_2PO_4^-$, HPO_4^{2-}, SO_4^{2-}, NO_2^-, NO_3^-, or CO_3^{2-}. The resistance performance is 10 to 100 times more efficient than SAMs containing all other tested anions.

Introduction

Perchlorate salts are an emerging persistent pollutant that potentially threatens human health by impairing the thyroid gland's function (hypothyroidism) upon long-term exposure.[1,2] Thyroid malfunctioning is caused by perchlorate competing with iodide binding to the thyroid's iodine receptors leading to hypothyroidism and fatal retardation, especially in developing infants and children. Perchlorate salts are highly soluble in water, sorb poorly to mineral or organic surfaces,[3] and are easily transferred to the ground and natural water reservoirs, resulting in soil contamination and enhanced levels of perchlorate in plants and food products.[4] The primary sources of perchlorate pollution arise from its extensive use as an oxidizer in the propellant industry, agriculture fertilizers, and automobile industry.[5] Therefore, sensitive perchlorate monitoring methods are increasingly needed to assess exposure and risks.[6]

A wide range of analytical methods is commonly used for perchlorate detection, including UV/Vis spectroscopy,[7] integrated mass spectrometry, such as ion or liquid chromatography-MS,[8–10] ion-exchange chromatography,[11,12] capillary electrophoresis,[13] and selection of staining assays.[14] More advanced analytical methods for perchlorate residues include ion-selective electrodes equipped with ion carriers within polymer membranes, total reflection X-ray fluorescence[15] and organism-based biosensors.[16] Overall, several methods are not target-specific or poorly quantifiable in the presence of other background ions, and some technologies require costly instruments and well-controlled experimental conditions. Hence, there is a need to develop highly selective, accessible methods.

Electrochemical determination of ion concentrations in aqueous solutions that employ self-assembled monolayers (SAMs) is advantageous because the easily prepared SAMs can cover metal electrodes.[17–19] SAMs with stable, densely packed,

[a] Dr. R. Khurana, Prof. O. Reany
Department of Natural Sciences
The Open University of Israel
1 University Road, Ra'anana, 4353701 (Israel)
E-mail: oferre@openu.ac.il
[b] Prof. J. Huskens
Molecular Nanofabrication Group, MESA + Institute
Faculty of Science and Technology
University of Twente
Drienerlolaan 5, 7522 NB Enschede (The Netherlands)
E-mail: j.huskens@utwente.nl
[c] Prof. E. Keinan
Faculty of Chemistry
Technion-Israel Institute of Technology
Technion, Haifa (Israel)
E-mail: keinan@technion.ac.il
[d] F. Alami, Prof. C. A. Nijhuis
Hybrid Materials for Opto-Electronics Group, MESA + Institute
Faculty of Science and Technology
University of Twente
Drienerlolaan 5, 7522 NB Enschede (The Netherlands)

Supporting information for this article is available on the WWW under https://doi.org/10.1002/chem.202302968

Special Collection Part of a Special Collection celebrating the 120th anniversary of the Royal Netherlands Chemical Society.

and well-defined structures can be achieved from either the solution or the gas phase.[20–24] Such analyte-specific SAM-based sensors require the incorporation of the appropriate receptor. A wide variety of selective receptors based on host–guest chemistry include cyclodextrins (CDs),[25–27] crown ethers,[28,29] calixarenes,[30,31] cucurbit[n]urils (CB[n]s),[32] pillarenes,[33] and bambus[6]urils (BU[6]s).[34] Although cation-detecting sensors based on SAMs have been developed, anion-detecting SAMs have remained challenging.

The new family of organic-soluble BU cavitands offers attractive opportunities as anion hosts.[35,36] Furthermore, replacing their portal ureido oxygen atoms with either sulfur or nitrogen produced various *hetero*-BU[6] molecules, such as *semithio*-BU[6] or *semiaza*-BU[6]s.[37] These new variants exhibited variable binding modes,[38–41] demonstrating channel-like, multiple anions binding,[41] and efficient transmembrane chloride transport.[42,43] Sindelar and co-workers have recently demonstrated the ionophore behavior of dodecabenzylbambus[6]uril (Bn_{12}BU[6]) embedded within a conducting polymer (PEDOT) in a solid-contact ion selective electrode (SC-ISE) and employed it to determine perchlorate concentrations at a μM level.[44] Although conducting polymers improve the durability, stability, and sensitivity of ISEs, the accumulation of a water layer at the electrode-membrane interface challenges the practical use of this method.[45]

An earlier study showed that anchoring *semithio*-BU[n] (n = 4, 6) to an Au surface forms self-assembled monolayers with strong interactions between the thiocarbonyl groups and the metal surface.[34] Unfortunately, while the electrochemical measurements proved that electron transfer occurred through the SAMs, and XPS confirmed that thiocarbonyl sulfur atoms were chemisorbed to the Au(111), forming ordered domains of SAMs, the molecules underwent large conformational changes that optimized their layer formation but reduced their anion binding.

Here we report that *semiaza*-BUs containing surface anchoring groups, such as thioether or disulfide entities, form SAM-based electrochemical anion sensing layers (Figure 1). As the bound BUs preserve their cavity conformation, they serve as selective anion receptors within the electrode-bound SAM. We demonstrate their anion recognition by impedance spectroscopy using a negatively charged redox mediator. Specific binding of an anion within the SAM-modified Au electrode repels the charged redox mediator, thus increasing the charge-transfer resistance. This phenomenon allowed comparing the affinity of various anions to the *semiaza*-BU SAMs at the electrode-solution interface. Furthermore, the method allowed increasing the sensitivity of anion detection down to the mM range by varying their thickness within 2.6 ± 0.6 nm. We observed up to three orders of magnitude preferential binding of perchlorate anions over F^-, Cl^-, I^-, AcO^-, $H_2PO_4^-$, HPO_4^{2-}, SO_4^{2-}, NO_2^-, NO_3^-, and CO_3^{2-}.

Results and Discussion

Synthesis

All *semiaza*-BU[6] derivatives were prepared using our previously reported one-pot, two-step synthesis, starting with the tetrabutylammonium bromide complex of *semithio*-BU[6], **1** (Scheme 1).[41] Thus, the reaction of **1** with methyl triflate at room temperature produced *semi*-(methyl)sulfonium-bambusuril, **2**, in the form of its triflate salt. The latter was reacted with various primary amines to give the corresponding *semiaza*-BU[6]s **3a–e** in 68–83% overall yields. These protonated compounds were neutralized, affording the free bases, **4a–e**, in nearly quantitative yields. Compounds **3e** and **4e** were reacted with succinic anhydride to produce the corresponding succinic acid monoester, **3f**, and its neutral form, **4f** (see below).

The solid-state structure of **3a**, crystallized from acetonitrile, exhibits an alternate arrangement of the *semiaza*-glycoluril units (Scheme 1, *Right*). The central anion-binding site comprises twelve methine hydrogens maintaining tight interactions with the bromide anion at the cavitand center. The most remarkable feature of this structure is the simultaneous

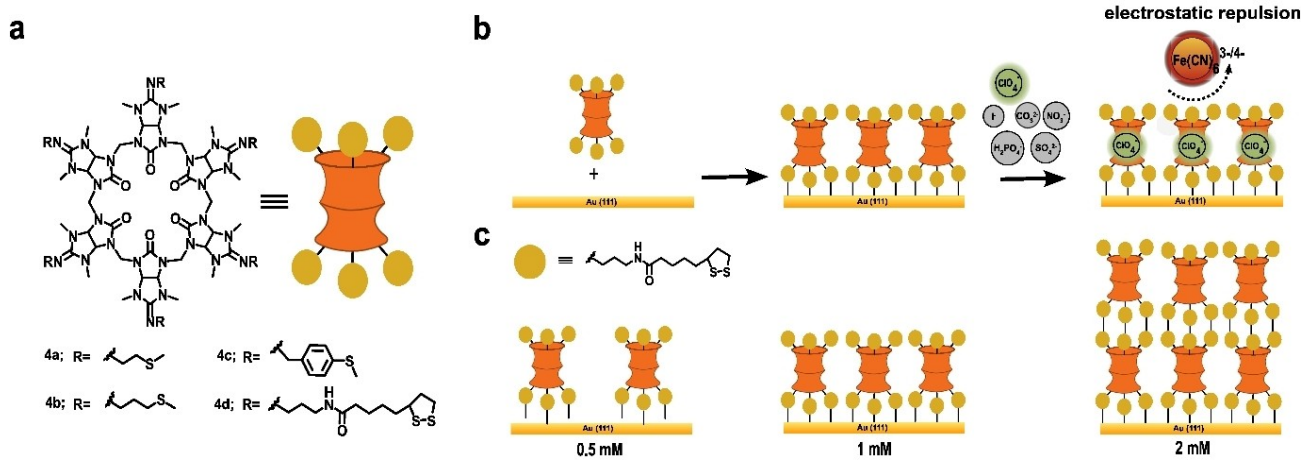

Figure 1. Schematic representation of *semiaza*-bambusuril-based self-assembled monolayers (SAMs) as electrochemical anion sensing electrodes: **A**. The structure of *semiaza*-BU[6] derivatives studied in this work. **B**. Formation of the SAM as a selective anion recognition layer. **C**. Proposed SAM architectures of **4d** formed as a function of the BU concentration used to make the SAMs.

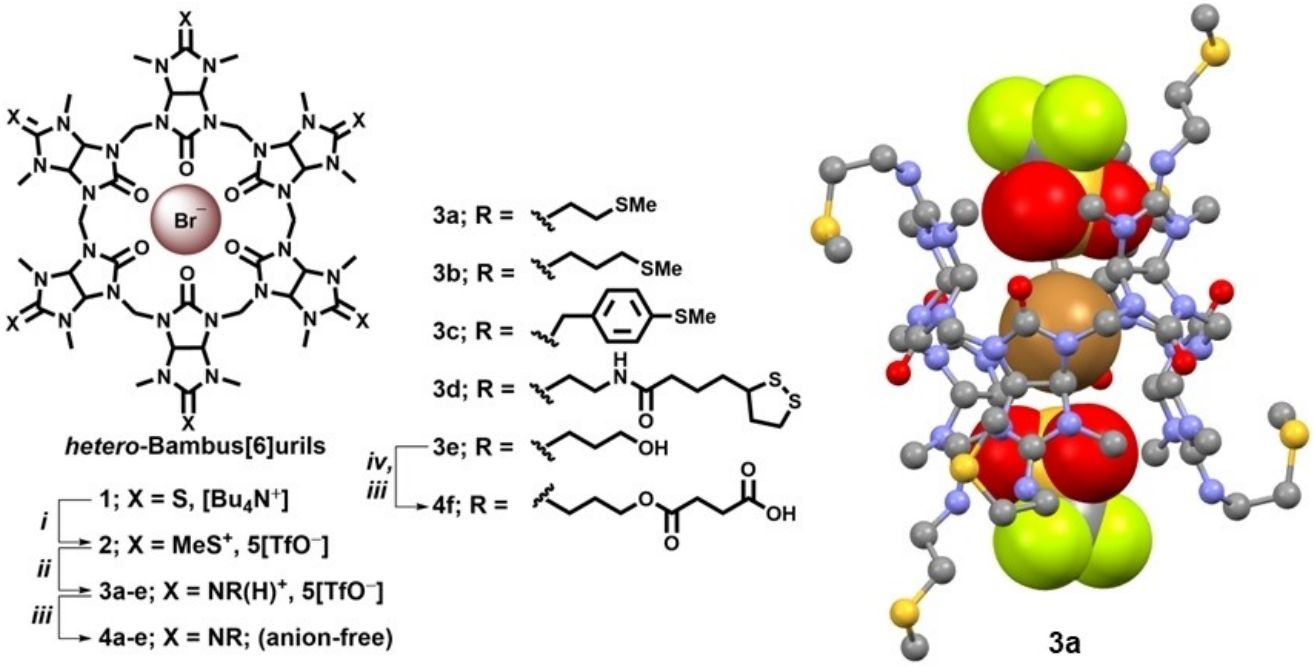

Scheme 1. *Left:* Synthesis of *semiaza*-BU[6] derivatives. Reagents and conditions: (i) MeOTf, DCM, *RT*, 2 h (80%); (ii) RNH_2, THF, reflux, 14 h (70%); (iii) Amberlyst A26 (OH^- form), MeOH, 15 min. (>95%); (iv) Succinic anhydride, NEt_3, DMAP, THF, reflux, 24 h. *Right:* Solid state structure of *semiaza*-BU[6], **3a** hosting one bromide and two triflate anions. Additional disordered solvent molecules and anions scattered in the void packing space were omitted for clarity. A Ball & Stick model represents the hosts, whereas the anions are represented by a Space-Filling model (oxygen, red; nitrogen, blue; fluorine, yellow; carbon, grey; bromine, brown; and sulfur, deep yellow).

accommodation of multiple anions, two triflates, and one bromide linearly positioned along the main symmetry axis of the host. The inter-anionic distances are remarkably short, 4.02 Å, reminiscent of the inter-anionic distance (4 Å) reported for adjacent chloride binding sites in the crystal structures of mutant E. coli ClC chloride channels.[46]

ITC study

We used isothermal titration calorimetry (ITC) to study the anion-binding properties of water-soluble *semiaza*-BU[6], **4f**, in aqueous solutions. Thus, solutions of **4f** in 100 mM KCl were used to maintain the ionic strength of both the host and the guest solutions and for comparison under the same conditions used in electrochemical impedance spectroscopy (EIS) studies (see below). The solutions of **4f** were titrated by a solution of MX salts (M=Na or K; X=ClO_4^-, I^-, CO_3^-, and NO_3^-) at 298 K (Table 1 and Figures S20-S21). All ITC curves were fitted to a single-step binding model (Figures S20 and S21). The entropy component ($T\Delta S°$) and binding free energy ($\Delta G°$) were derived from the experimental values of the association constant (K_a) and the enthalpy ($\Delta H°$) (Table 1).

The thermodynamic values obtained for the various anions reveal two distinct groups, the weakly hydrated, isotropically shaped anions, perchlorate (tetrahedral), and iodide (spherical) ($\Delta G_h = -102.7$ and -65.7 kcal/mol, respectively), and the more anisotropically shaped, hydrated anions, nitrate, and carbonate (both exhibit trigonal planar shape with $\Delta G_h = -71.6$ and -314.1 kcal/mol, respectively).[47] The ITC results indicate that the anion-binding exchange process with the first group is enthalpy-driven, accompanied by minor negative (unfavorable) entropy change. Conversely, with the more anisotropically shaped, hydrated anions, both enthalpy and entropy contribute to the binding affinities between **4f** and the anions. Guest binding is dominated by significant negative enthalpy change

Table 1. Binding constants and thermodynamic parameters elucidated from ITC data of **4f** titrated with different anions in 100 mM KCl, at 298 K.[a]

Anion	*n*	K_a [M^{-1}, $\times 10^5$]	$\Delta G°$ [kcal/mol]	$\Delta H°$ [kcal/mol]	$T\Delta S°$ [kcal/mol]
ClO_4^-	1	4.08 ± 0.24	−7.65 ± 0.03	−8.19 ± 0.04	−0.54 ± 0.01
I^-	1	1.44 ± 0.03	−7.05 ± 0.11	−7.20 ± 0.02	−0.17 ± 0.01
CO_3^{2-}	1	0.50 ± 0.06	−6.41 ± 0.08	−3.39 ± 0.09	3.02 ± 0.02
NO_3^-	1	0.06 ± 0.01	−5.13 ± 0.12	−3.50 ± 0.37	1.63 ± 0.25

[a] Data analyzed by a one-site fitting model. Errors obtained from curve fitting.

($\Delta H°$) for host–guest complexation with both anion groups. We have previously attributed the host–guest interactions to induced dipoles at the bambusuril host and the attractive charge transfer interactions between the anion-filled orbitals and the σ* of the methine C–H and C–N bonds.[48]

The positive entropy changes ($T\Delta S°$) reflect the conformational rigidity of the host and desolvation of the anion guests. Compensation for this effect by releasing the high-energy water molecules from the bambusuril cavity is more pronounced than for isotropically shaped, weakly hydrated anions.[49] Overall, the perchlorate and iodide anions show higher binding affinities to the water-soluble derivative, **4f**, and significantly weaker binding with nitrate and carbonate, in agreement with a similar trend found in previously reported water-soluble BU[6] derivatives.[35]

SAM Preparation and Characterization

CV measurements

SAMs of **4a–d** on gold electrodes were prepared by immersion of freshly cleaned bare gold electrodes to solutions of **4a–d** (1 mM) in EtOH:DMSO (4:1) overnight in the dark under N_2. After rinsing the SAM-modified gold electrodes with copious EtOH:DMSO (4:1) and drying under a stream of N_2, they were characterized by recording their cyclic voltammograms (CVs). Their current blocking effect was determined by their electrochemical response to the $Fe(CN)_6^{3-/4-}$ redox probe (Figure 2).

Reversible redox behavior with $E_{1/2} = 0.24$ V vs. Ag/AgCl was observed on bare gold electrodes (Figure 2A, black line). In comparison, attenuation of the current, especially the anodic current, reveals that SAMs of **4a–d** were formed on the electrode surfaces, partially blocking the redox process of $Fe(CN)_6^{3-/4-}$. Accordingly, the peak anodic current values for SAMs of **4a** and **4b** ($i_{p,a}$) are only reduced by 11.5% ($i_{p,a}$ = 0.101 mA) compared to that of the bare gold electrode (0.114 mA), indicating minor blocking of the $Fe(CN)_6^{3-/4-}$ redox probe. However, the SAMs of **4c** and **4d** exhibit lower current values (0.077 and 0.031 mA), presenting a significant blocking effect of approx. 32% and 74%, respectively (Figure 2A green and purple lines). The different blocking effects may reflect the packing modes of the SAMs and/or redox-couple permeability through the monolayers.

Remarkably, SAMs prepared by immersion of the gold electrode within different concentrations of **4d** (Figure 2B) showed a strong dependence on the BU concentration during the SAM preparation from the solution. At 0.5 mM, hardly any blocking occurred, while SAM preparation from 2 mM solution resulted in almost complete blockade.

XPS studies

X-ray photoelectron spectroscopy (XPS) is a powerful tool for showing the presence of adsorbate molecules on a surface and investigating the interactions at the interface between the anchoring groups and the metal substrate. Moreover, the average fractions of bound headgroup to the metal surface can be estimated by probing the chemistry occurring at the headgroup-metal interface in SAMs deposited onto a "flat" metal surface. Indeed, the XPS measurements identified the core level binding energy spectra of the substrate (*Au*4f), carbon (*C*1s), nitrogen (*N*1s), and sulfur (*S*2p) in **4a**-, **4c**- and **4d**-based SAMs (Figures S23–S26). Table S2 provides the binding energies (BE), full-width at half-maxima (FWHM), and relative intensity ratios.

Expectedly, *Au*4f spectra were composed of spin-orbit doublet ($Au4f_{7/2}$) with the more intense $Au4f_{7/2}$ component (BE = 82.9–84.8 eV), due to metallic Au(0) atoms, which were taken as a reference. The spin-orbit pair at higher BE values (86.5–88.5 eV) is associated with Au(I) atoms covalently bonded

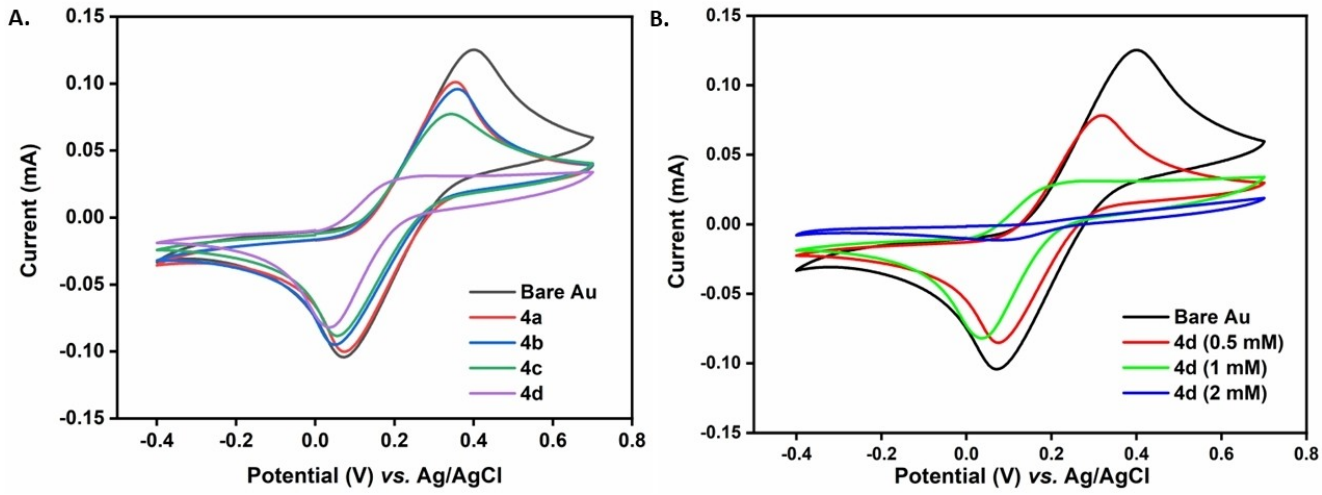

Figure 2. Cyclic voltammograms of $Fe(CN)_6^{3-/4-}$ (1 mM) in water with KCl (0.1 M) as supporting electrolyte at the bare gold electrode and SAM-modified gold electrodes: **A**. bare gold (black), **4a** (red), **4b** (blue), **4c** (green) and **4d** (purple) monolayers. **B**. SAM-covered gold electrodes produced under various **4d** concentrations: 0.5 mM (red), 1.0 mM (green) and 2.0 mM (blue). The scan rate was 100 mV s^{-1} in the potential range from −0.4 to 0.8 V.

to the terminal sulfur groups of either thioether or disulfide ligands. Remarkably, we observed an increasing attenuation factor in the Au band, indicating a higher thickness of the **4d** layers (made at 1 mM) than **4c** than **4a** (see Table S3). The collected XPS spectra of *C1s* were deconvoluted into three components at 284.7 (only for **4a**), 286.5, 287–288 and 289–290 eV (only for **4c** and **4d**), which are assigned to C–C, C–S and C=O species, respectively. Likewise, the collected XPS spectra of *S*2p showed multiple doublets corresponding to chemisorbed or physisorbed S–Au.[50] Accordingly, the binding energies within the range of 158–172 eV were deconvoluted using the *S*2p doublet with a branching ratio of 2:1 and an energy difference of 1.2 eV of the spin-orbit pair $S2p_{3/2}$–$S2p_{1/2}$. For all SAM samples, two surface species were predominant: gold-bound sulfur, with *S*2p3/2 (*S*2p1/2) at 161.1 (162.3) for **4a**,163.0 (164.2) for **4c** and **4d**, and 161.9 (163.1) eV for **4d** (0.5 mM). The binding energies for unbound sulfur with *S*2p3/2 (*S*2p1/2) were indicated at 163.0 (164.2) for **4a**, 165.1 (166.3) for **4c**, 164.8 (166.0) for **4d**, and 163.8 (165.0) eV for **4d** (0.5 mM). Remarkably, the typical band representing the oxidized form of sulfur (Table S2, *S*2p band for S–Ox) was absent from the *S*2p region of **4d**-based SAMs, suggesting excellent stability of the lipoic amide ligand on the gold surface.[51]

We also determined the fraction of sulfur anchoring groups that participated in binding to the metal surface for each analyzed SAM by summing the integrals of both bound and unbound *S*2p bands. For example, in the XPS spectra of **4a**, the calculated value obtained for the bound sulfur was 61% (Table 2), implying that sulfur atoms at both rims are involved in binding to the Au surface and suggesting less dense layers with potentially complete loss of anion binding affinity.[34] In contrast, a smaller fraction of bound S–Au was observed in the XPS spectra of SAMs of **4c** (36%), inferring that only one rim is involved in the assembly process onto the gold surface. The attenuation of the bound sulfur signal caused by the location of these atoms at the bottom of the SAM may explain the $<50\%$ value observed here.

With SAMs of **4d** prepared by immersing the bare gold electrode in 1 mM solution of **4d**, the bound S–Au fraction dropped to 19%. Even for SAMs prepared with a more dilute solution (0.5 mM), the calculated value (28%) was less than that of **4c**. These lower values are in line with the occurrence of thicker layers, possibly caused by interchain crosslinking of the lipoic acid functionalities (see below), of which a smaller fraction of the S atoms is directly bonded to Au and at the same time buried more deeply inside the layer.

Table 2. SAM surfaces characterized by XPS, ellipsometry (thickness), AFM (roughness) and contact angle measurements.

SAMs[a]	bound S [%][b]	thickness [nm]	RMS roughness [nm][c]	θ_a [°]
4a	61			60
4c	36	36	2.2 ± 0.3	51
4d (1 mM)	19	19	3.1 ± 0.1	42
4d (0.5 mM)	28	28	2.3 ± 0.1	46

[a] Unless otherwise mentioned, the SAMs were prepared in 1 mM solutions of **4a-d**. [b] Percentage of sulfur bound to Au, as determined by XPS. [c] RMS = root mean square. The error values on the ellipsometry data correspond to a single standard deviation obtained from 3 measurements performed at different angles (see Supporting Information).

Combining the XPS results with the resulting CV data (Figure 2B) obtained for SAMs of **4d** at three different concentrations, the effect of interchain crosslinking[52] in the packing structure on the gold surface cannot be ignored. Thus, the lipoic amide with its active dithiolane ring structure tends to form more than one bond to the metal substrate because the S–S disulfide bond (as a physisorbed ligand) can be reduced spontaneously on the Au surface to form Au–S bonds as chemisorbed bidentate ligand.[50] Additionally, the above-described intercrossing process may involve disulfide metathesis between headgroups of adjacently adsorbed molecules. This phenomenon is well documented in core crosslinked micelles[53–56] and nanoparticles[57] but has never been discussed in the context of SAM-based sensors. In our SAMs of **4d**, lipoic acid moieties of one rim only are involved in binding to the gold surface, allowing the free groups of the other rim to engage in intercrossing.

Ellipsometry measurements

Ellipsometry measurements were performed to assess the layer thicknesses of SAMs made of **4c** and **4d** (Tables S4-S6). The thickness of **4c** SAM was found to be nearly 2.2 nm (Figure S27), comparable with the extended length of the **4c** molecule (2 nm). This finding supports the formation of a monolayer on the Au electrode. As anticipated, the thickness of the **4d** SAMs increased with the concentration of 4d in the mother solution. With 0.5 mM, the calculated thickness of the layer was 2.3 nm (Figure S28), whereas with 1 mM, a thicker layer of 3.1 nm was measured (Figure S29), in agreement with the extended size of **4d** (3.2 mm). Hence, the recorded thickness of a SAM produced from a mother solution of 0.5 mM suggests that the deposition and growth mode of the monolayer is imperfect, whereas a well-ordered monolayer of **4d** was formed with solutions of 1 mM. The SAMs formed in a 2 mM solution of **4d** showed an inhomogeneous thickness, which could not be assessed properly by the available model.

AFM study. For further characterization of representative SAMs, the surface topography was analyzed by AFM to give images with a scan area of 1.0 μm ×1.0 μm, and the RMS roughness values were measured (Table 2 and Figure S22). For **4d** SAMs, an increase in the surface roughness was observed from **4d** SAM formed in 0.5 mM (0.82 nm) to **4d** SAMs formed in 1.0 mM solution (1.17 nm). In contrast, the RMS roughness of **4c** SAMs was significantly smaller (0.63 nm). We attribute the significant increase in surface roughness of both types of **4d** SAMs to increased interchain crosslinking of the disulfide groups. The AFM images of these SAMs also showed no aggregates, indicating a good surface coverage of a densely packed film. Last, we characterized the various SAMs using

water contact angle measurements. All SAMs formed moderately wettable surfaces, $\theta_a = 42\text{-}60°$ (Table 2), indicating that SAMs bearing thioether and disulfide groups have comparable hydrophobicity. The contact angle with **4a** stands out, probably due to its relatively high hydrophobicity.

Electrochemical anion binding studies

We focused on perchlorate for the cyclic voltammetry experiments because ITC measurements showed a high binding affinity of this anion to **4f**. We assessed the perchlorate sensing properties of **4a--d** as SAMs on gold electrodes in the presence of 10 to 100 mM of sodium perchlorate (Figure 3). Well-defined characteristic peaks of the redox couple, $Fe(CN)_6^{3-/4-}$ on the bare gold electrode were observed. For SAM-modified Au electrodes with **4a** or **4b**, the anodic and cathodic peaks were retained even at 100 mM perchlorate anion (Figure 2A and B). We attribute these results to the negligible blocking effect of ClO_4^-, possibly due to the low coverage of the Au surface by **4a** or **4b** or a low affinity of these BUs' SAMs to perchlorate. However, in SAM-modified Au electrodes with **4c** or **4d** formed under three different concentrations, the redox peaks were noticeably reduced, confirming perchlorate binding to the BU's cavity, thus enhancing the repulsion of the redox couple from the gold surface and quenching the expected Faradaic current.

For SAMs of **4c** or **4d** formed in 0.5 mM solution (Figure 3C and D), the Faradaic current gradually disappeared upon a significant increase in the perchlorate concentration up to 2 M. These results might indicate imperfect coverage of both **4c** formed in 1 mM, and **4d** formed in 0.5 mM solution. In contrast, with SAMs of **4d** formed in 1 mM (Figure 3E), the Faradaic current was completely blocked at 600 mM of ClO_4^-, indicating optimal layer coverage of the gold electrode. Notably, with SAMs of **4d** formed in or 2 mM (Figure 3F), the current was blocked at a concentration as low as 28 mM of ClO_4^-, suggesting higher resistivity of an interchain crosslinked layer, already saturated with perchlorate anions at low concentrations.

Electrochemical impedance spectroscopy measurements

Following the perchlorate binding behavior, with the best performance of **4d** SAM as a sensitive sensor, we employed electrochemical impedance spectroscopy (EIS) to gain deeper insight and quantify the anion recognition properties at the electrode surface in the presence of various anions. Accordingly, the electron transfer process can be affected between the electrode and the redox couple $Fe(CN)_6^{3-/4-}$ in electrolyte solutions during the binding of an anion to the SAM receptor. The electrostatic repulsion between the negatively charged SAM surface and the soluble negatively charged redox couple increases the charge transfer resistance of the redox probe in solution. Figure 4 shows the complex impedance responses of 1 mM $Fe(CN)_6^{3-/4-}$ at a SAM-modified gold electrode prepared in 1 mM **4d** in the presence of various anions. The impedance of $Fe(CN)_6^{3-/4-}$ was recorded with the addition of 100 mM of F^-, Cl^-, I^-. NO_3^-, NO_2^-, CO_3^{2-}, SO_4^{2-}, HPO_4^{2-}, $H_2PO_4^-$, AcO^-, and ClO_4^- as the electrolyte anions. The Nyquist plots of all the

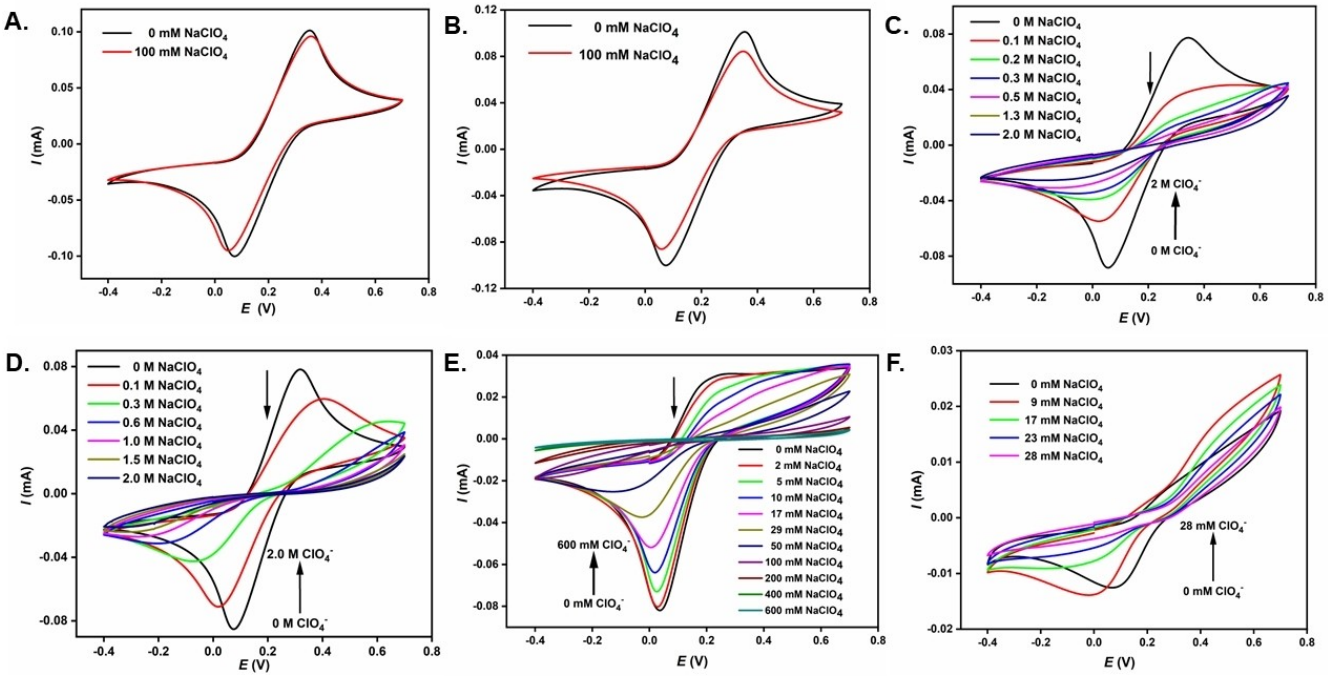

Figure 3. Cyclic voltammograms of $Fe(CN)_6^{3-/4-}$(1 mM) in KCl (0.1 M) as supporting electrolyte at gold electrodes covered with SAMs of **4a-d** in the absence (black) and presence (colours) of sodium perchlorate ($NaClO_4$). All CVs were scanned at a rate of 100 mV s^{-1} in the potential range from −0.4 to 0.8 V. **A** and **B**. CV plots of SAMs of **4a** and **4b**, respectively, before and after adding 100 M ClO_4^-. **C**. CV plot of **4c** in the presence of increasing amounts of $NaClO_4$. **D-F**. CV plots of **4d** SAM formed at three different concentrations (0.5, 1, and 2 mM, respectively) before and after incremental additions of $NaClO_4$.

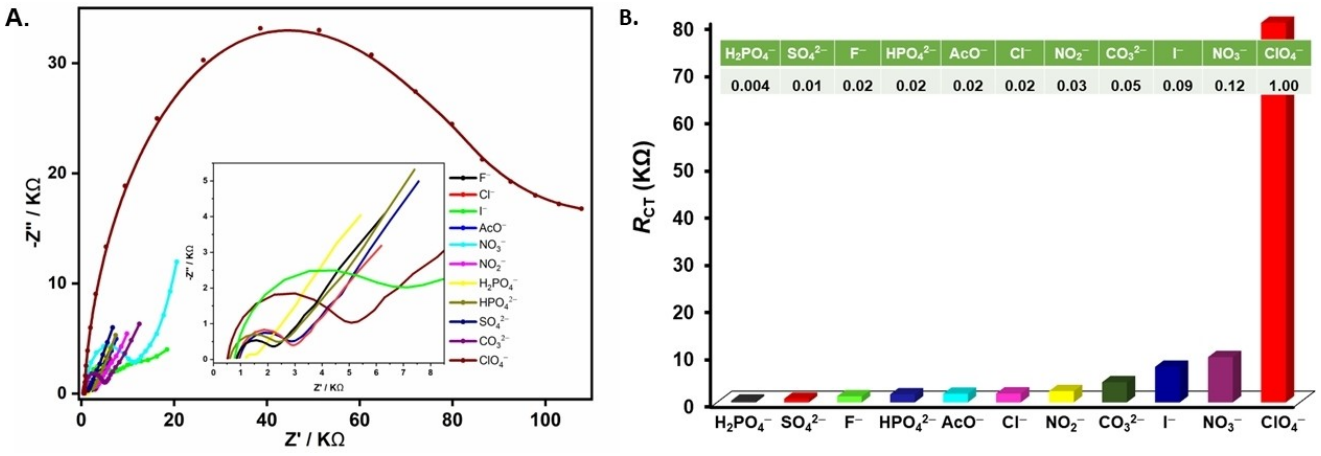

Figure 4. Anion recognition properties of **4 d** monolayers by EIS using $Fe(CN)_6^{3-/4-}$ as a redox probe. **A**. Impedance response at the bilayer-coated Au electrodes of compound **4 d** (1 mM) in the presence of different anions (100 mM) (frequency range from 10 kHz to 10 MHz). The inset contains selected EIS spectra following a fast electrode reaction. **B**. A bar diagram comparing the maximum charge transfer resistance (R_{CT}) values obtained from fits to Randle's equivalent circuit (Table S4). The inset table lists the selectivity factors calculated as the ratio of the measured R_{ct} of all anions to that of perchlorate. Error values (< 10%) correspond to an average of 3 measurements.

anions, except ClO_4^-, follow only a part of a semicircle with Warburg impedance (Figure 4A), which reveals a low charge transfer resistance, indicative of little to no anion binding.

The SAM-modified gold electrode exhibited a relatively very low charge transfer resistance (R_{CT}) in the presence of 100 mM solutions of $H_2PO_4^-$, SO_4^{2-}, F^-, HPO_4^{2-}, AcO^-, Cl^- or NO_2^- (Table S4, R_{ct} < 3 kΩ), indicating that the residual resistance is mainly due to the densely packed organic SAMs and that these anions do not bind appreciably to the SAM receptors either in solution or on the modified surface of the gold electrode. In all cases, the Nyquist plots obtained on the SAM-modified gold electrode display mainly a Warburg impedance (Z_W, a straight line) because there is no blocking effect, and consequently, a fast charge transfer reaction on the electrode surface occurs, limited by diffusion of the redox couple. Adding anions to the SAM-modified gold electrode, such as I^-, NO_3^-, or CO_3^{2-} (100 mM), resulted in small R_{CT} values (7.5, 9.6, and 4.3 kΩ).However, upon adding 100 mM ClO_4^- to the SAM-modified gold electrode, a remarkable change in the R_{CT} was measured (80.2 kΩ), demonstrating the strong affinity of perchlorate anion to the **4 d** SAM-modified gold electrode and high binding selectivity (Figure 4B). Hence, the blocking effect is the main factor for such high charge transfer resistance. The resistance performance with perchlorate is 10 to 100 times more efficient than with SAMs containing all other tested anions. These results are also aligned with the above-described ITC measurements.

When the probe was changed to a positively charged one, $Ru(NH_3)_6^{3+/2+}$ (1 mM), the R_{CT} values decreased instead of increased, from 251 kΩ in the absence of ClO_4^- to 49 kΩ in the presence of 100 mM of ClO_4^- (Figure S27 and Table S5), thus confirming the accumulation of a negative surface charge upon anion binding. The impedance responses obtained by employing negatively and positively charged redox couples indicated that selective perchlorate anion binding occurred on the gold electrode surface with SAMs of **4 d**.

Next, the impedance responses of 1 mM $Fe(CN)_6^{3-/4-}$ at the 1 mM **4 d** monolayer-modified gold electrode were recorded in the absence and presence of increasing concentrations of ClO_4^-. The R_{CT} values increased from 0.67 kΩ in the absence of ClO_4^- to a maximal value of 302 kΩ in the presence of 400 mM ClO_4^- (Table S9). This trend of gradual enhancement in the SAM-modified electrode resistance indicated that interfacial electron transfer from the electrode to the redox probe was inhibited with increasing perchlorate concentrations. A consistent phenomenon was also shown by CV: with increasing concentrations of ClO_4^-, the peak currents were lower than those in the absence of ClO_4^- (Figure 3E).

The interactions between the anion receptors **4 c** and **4 d** with perchlorate at the interface between the gold electrode and the bulk solution can be further understood if the equilibrium constant is expressed as the association constant (K_a). At a given perchlorate concentration, the SAM can be viewed with as many parallel electrodes as possible, each with a cavity, part unbound and the other bound. This viewpoint provides the following equation:

$$\frac{1}{R_{CT}} = \frac{\theta_{ub}}{R_{CT,ub}} + \frac{\theta_b}{R_{CT,b}} \quad (1)$$

Where θ_{ub} and θ_b are the surface densities of unbound and bound cavities, respectively, while $R_{CT,ub}$ and $R_{CT,b}$ are the corresponding charge-transfer resistances. K_a can then be fitted to the data by noting that:

$$K_a = \frac{\theta_b}{\theta_{ub}[ClO4]} \quad (2)$$

The dependence of R_{CT}^{-1} on perchlorate concentration presented in Figure S31A and Figure 5A–B following the addition of perchlorate at various concentrations to **4 c** and **4 d**, respectively, allowed us to determine (Figure S31B and Fig-

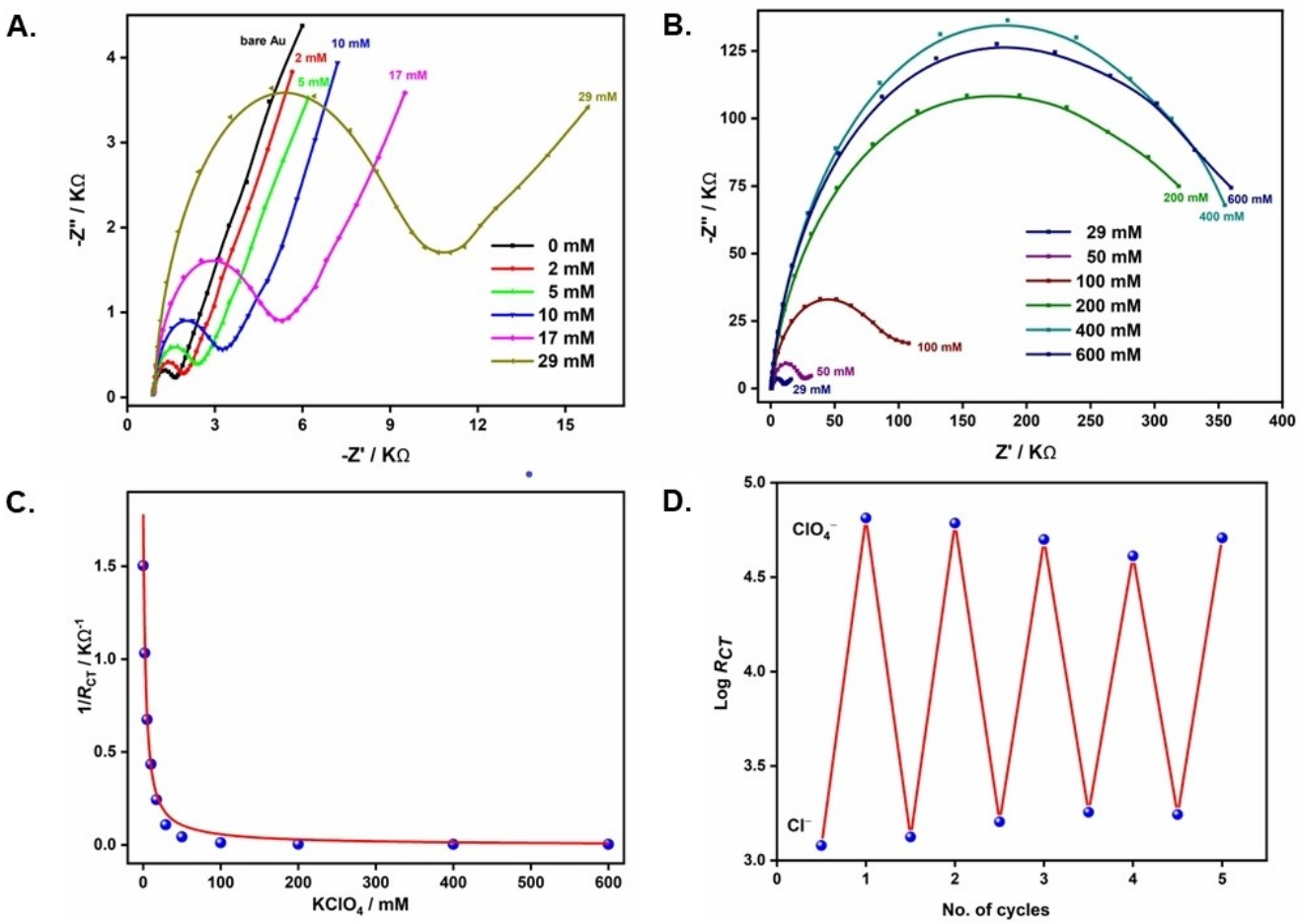

Figure 5. Impedance spectra at **4 d**-SAM modified Au electrode after sensing perchlorate anion in the presence of $Fe(CN)_6^{3-/4-}$ for **A**. 0–30 mM and **B**. 30–600 mM of $NaClO_4$. **C**. A plot of the corresponding reciprocal charge transfer resistance (R_{CT}^{-1}) with perchlorate concentration. **D**. Detection of perchlorate anions (100 mM) in five consecutive runs.

ure 5C) the binding constants (150 and 350 M^{-1}, respectively). These values are considerably lower than the affinities observed in the solution (ITC data, see above). It may be attributed to the closeness of the metal surface to the anion and some change of the cavity's conformation upon SAM formation, affecting the anion binding.

Nevertheless, these SAMs provide the first BU examples for preserving anion binding. The similar equilibrium binding data (Table 3) indicate that both SAM-modified gold electrodes exhibit identical cavities. Since **4 d** is a more densely packed film than **4 c**, SAM **4 d** is a more sensitive perchlorate sensing layer of order of magnitude. **4 d** (1 mM) films can sense 2 mM perchlorate, whereas, with **4 c**, the modified electrode can sense 20 mM perchlorate.

To test the performance stability of the SAM-modified Au electrode, we immersed the SAM-modified Au electrode in KCl (100 mM) solution. We determined the R_{CT} from the impedance response curve. Then, the electrode was thoroughly washed with copious doubly deionized water (DDW). Finally, the electrode was immersed in 100 mM $NaClO_4$ solution, and the impedance response curve was recorded to provide the corresponding R_{CT}. We repeated this experiment over five cycles, recording the R_{CT} in the presence of perchlorate anions with an average value of 65 kΩ and R_{CT} with an average value of 1.3 kΩ in the presence of chloride (Figure 5D), demonstrating the stable performance of the SAM-modified Au electrode. The high selectivity towards perchlorates allows us to use this model sensory device with high selectivity/sensitivity and reuse it multiple times with potentially continuous, real-time perchlorate monitoring under flow conditions.

Table 3. Binding constants and charge transfer resistance (R_{CT}) of perchlorate-bound SAM-modified Au electrodes with either **4 c** or **4 d** (1 mM) as elucidated from EIS data at 298 K.

SAM-modified Au electrode	n	K_a [M^{-1}, $\times 10^2$]	R_{CT} (bound) [kΩ]	R_{CT} (unbound) [kΩ]
4 c	1	1.5	24.3	0.16
4 d	1	3.5	274	0.66

Conclusions

Self-assembled monolayers (SAMs) of *semiaza*-BU[6] derivatives bearing thioethers or dithiolane ring as anchoring groups on gold surfaces were prepared. All SAMs were characterized by cyclic voltammetry with $Fe(CN)_6^{3-/4-}$ as a redox probe, X-ray photoelectron spectroscopy (XPS), atomic force microscopy (AFM), and ellipsometry, revealing that *semiaza*-BUs equipped with benzyl methyl thioether (**4c**) and especially the lipoic amide group (**4d**) are suitable for anion sensing measurements. Both derivatives bind perchlorate preferentially over other anions such as F^-, Cl^-, I^-, AcO^-, $H_2PO_4^-$, HPO_4^{2-}, SO_4^{2-}, NO_2^-, NO_3^-, or CO_3^{2-} as indicated by electrochemical impedance spectroscopy (EIS) employing both negative and positively charged redox couples. Selective perchlorate anion binding occurs on the surfaces, consistent with the results obtained by the ITC study in aqueous solutions.

The use of EIS in this study demonstrates several advantages for anion sensing: (a) anion sensing can be easily conducted in aqueous systems, (b) anion sensors with stable cycling charge-transfer resistance performance can be achieved by assembling BU-based anion receptors to surfaces, and (c) SAMs bearing lipoic amide anchoring groups on the Au substrate allow for fine-tuning of anion detection sensitivity as a function of the SAM layer thickness and quality. Our laboratories aim to broaden the scope of semiaza-BUs to develop more selective and sensitive anion sensors.

Supporting Information

Experimental details describing the synthesis and characterization of all new compounds, including solution NMR assignments and crystal structure (CCDC 2240896), details of SAM characterization and anion binding studies (PDF).

Deposition Number(s) 2240896 (for **3a**) contain(s) the supplementary crystallographic data for this paper. These data are provided free of charge by the joint Cambridge Crystallographic Data Centre and Fachinformationszentrum Karlsruhe Access Structures service. The authors have cited additional references within the Supporting Information.[58-60]

Acknowledgements

We thank Dr. Natalia Fridman of the crystallographic lab at the Schulich Faculty of Chemistry, Technion, for her assistance in the crystallographic study of **3a**. The Open University of Israel team gratefully acknowledges the financial support from the joint research program of the Israel Science Foundation and the National Natural Science Foundation of China (ISF-NSFC grant No. 3665/21).

Conflict of Interests

The authors declare no conflict of interest.

Data Availability Statement

The data that support the findings of this study are available from the corresponding author upon reasonable request.

Keywords: anion sensing · bambusurils · electrochemical impedance spectroscopy · self-assembled monolayers · supramolecular chemistry

[1] R. A. Clewell, E. A. Merrill, L. Narayanan, J. M. Gearhart, P. J. Robinson, *Int. J. Toxicol.* **2004**, *23*, 17–23.
[2] J. Wolff, *Pharmacol. Rev.* **1998**, *50*, 89–105.
[3] B. A. Logan, *Environ. Sci. Technol.* **2001**, *35*, 482A-487A.
[4] W. E. Motzer, *Environ. Forensics* **2001**, *2*, 301–311.
[5] P. Dasgupta, J. Dyke, A. Kirk, A. Jackson, *Environ. Sci. Technol.* **2006**, *40*, 6608–6614.
[6] P. Niziński, A. Błażewicz, J. Kończyk, R. Michalski, *Rev. Environ. Health* **2021**, *36*, 199–222.
[7] H. Sun, Y. Liang, L. Zhou, X. Zhang, F. Luo, Z. Chen, *Anal. Sci.* **2022**, *38*, 525–531.
[8] J. Mathew, J. Gandhi, J. Hedrick, *J. Chromatogr. A* **2005**, *1085*, 54–59.
[9] S.-L. Lin, C.-Y Lo, M.-R. Fuh, *J. Chromatogr. A* **2012**, *1246*, 40–47.
[10] P. Constantinou, D. Louca-Christodoulou, A. Agapiou, *Chemosphere* **2019**, *235*, 757–766.
[11] D. M. West, R. Mu, S. Gamagedara, Y. Ma, C. Adams, T. Eichholz, J. G. Burken, H. Shi, *Environ Sci. Pollut. Res.* **2015**, *22*, 8594–8602.
[12] M. Lehmana, S. Badruzzamana, D. J. Adhama, D. A. Roberts, *Water Res.* **2008**, *42*, 969–976.
[13] P. I. Kubáň, K. Kiplagat, P. Boček, *Electrophoresis* **2012**, *33*, 2695–2702.
[14] K. H. Kucharzyk, R. L. Crawford, A. J. Paszczynski, T. F. Hess, *J. Microbiol. Methods* **2010**, *81*, 26–32.
[15] V. S. Hatzistavros, N. G. Kallithrakas-Kontos, *Anal. Chem.* **2011**, *83*, 3386–3391.
[16] S. A. Alsaleh, S. A. L. Barron, S. Sturzenbaum, *Anal. Methods* **2021**, *13*, 327–336.
[17] A. J. Hopkins, C. L. McFearin, G. L. Richmond, *J. Phys. Chem. C* **2011**, *115*, 11192–11203.
[18] M. A. Herranz, B. Colonna, L. Echegoyen, *Proc. Natl. Acad. Sci. USA.* **2002**, *99*, 5040–5047.
[19] B. Kaur, C. A. Erdmann, M. Daniels, W. Dehaen, Z. Rafinski, H. Radecka, J. Radecki, *Anal. Chem.* **2017**, *89*, 12756–12763.
[20] Y. Tong, G. R. Berdiyorov, A. Sinopoli, M. E. Madjet, V. A. Esaulov, H. Hamoudi, *Sci. Rep.* **2021**, *11*, 12772.
[21] S. Casalini, C. A. Bortolotti, F. Leonardi, F. Biscarini, *Chem. Soc. Rev.* **2017**, *47*, 40–71.
[22] C. Vericat, M. E. Vela, G. Corthey, E. Pensa, E. Cortes, M. H. Fonticelli, F. Ibanez, G. E. Benitez, P. Carro, R. C. Salvarezza, *RSC Adv.* **2014**, *4*, 27730–27754.
[23] G. A. Hudalla, W. L. Murphy, *Soft Matter.* **2011**, *7*, 9561–9571.
[24] F. Schreiber, *Prog. Surf. Sci.* **2000**, *65*, 151–256.
[25] J. Chen, X. M. Huang, C. Yan, H. Guo, Z. Gao, H. Shao, *Anal. Chim. Acta* **2020**, *1125*, 135–143.
[26] W. Zhan, T. Wei, Q. Yu, H. Chen, *ACS Appl. Mater. Interfaces* **2018**, *10*, 36585–36601.
[27] A. Méndez-Ardoy, T. Steentjes, T. Kudernac, J. Huskens, *Langmuir* **2014**, *30*, 3467–3476.
[28] S. Kumbhat, U. Singh, *J. Electroanal. Chem.* **2018**, *809*, 31–35.
[29] S. Flink, F. C. J. M. van Veggel, D. N. Reinhoudt, *Adv. Mater.* **2000**, *12*, 1315–1328.
[30] L. Troian-Gautier, A. Mattiuzzi, O. Reinaud, C. Lagrost, I. Jabin, *Org. Biomol. Chem.* **2020**, *18*, 3624–3637.
[31] Y. Cao, Z. Cao, J. Y. Xia, J. L. Zeng, L. X. Sun, *Adv. Mater. Res.* **2011**, *239–242*, 2054–2057.
[32] M. Wiemann, P. Jonkheijm, *Cucurbiturils and Related Macrocycles, Chap. 16 (Edn.: K. Kim), RSC*, **2020**, pp. 442–463.
[33] Y.-W. Yang, Y.-L. Sun, N. Song, *Acc. Chem. Res.* **2014**, *47*, 1950–1960.
[34] P. P. Kunturu, O. Kap, K. Sotthewes, P. Cazade, H. J. W. Zandvliet, D. Thompson, O. Reany, J. Huskens, *Mol. Syst. Des. Eng.* **2020**, *5*, 511–520.
[35] T. Lizal, V. Sindelar, *Isr. J. Chem.* **2018**, *58*, 326–333.
[36] J. Svec, M. Necas, V. Sindelar, *Angew. Chem. Int. Ed.* **2010**, *49*, 2378–2381.

[37] O. Reany, A. Mohite, E. Keinan, *Isr. J. Chem.* **2018**, *58*, 449–460.
[38] M. Singh, E. Solel, E. Keinan, O. Reany, *Chem. Eur. J.* **2015**, *21*, 536–540.
[39] P. Mondal, E. Solel, S. Mitra, E. Keinan, O. Reany, *Org. Lett.* **2020**, *22*, 204–208.
[40] P. Mondal, E. Solel, N. Fridman, E. Keinan, O. Reany, *Chem. Eur. J.* **2019**, *25*, 13336–13343.
[41] M. Singh, E. Solel, E. Keinan, O. Reany, *Chem. Eur. J.* **2016**, *22*, 8848–8854.
[42] R. Khurana, F. Yang, R. Khurana, J. Liu, E. Keinan, O. Reany, *Chem. Commun.* **2022**, *58*, 3150–3153.
[43] C. Lang, A. Mohite, X. Deng, Z. Dong, J. Xu, J. Liu, E. Keinan, O. Reany, *Chem. Commun.* **2017**, *53*, 7557–7560.
[44] P. Itterheimová, J. Bobacka, V. Šindelář, P. Lubal, *Chemosensors* **2022**, *10*, 115.
[45] Y. Lyu, S. Gan, Y. Bao, L. Zhong, J. Xu, W. Wang, Z. Liu, Y. Ma, G. Yang, L. Niu, *Membranes* **2020**, *10*, 128.
[46] R. Dutzler, E. B. Campbell, R. MacKinnon, *Science* **2003**, *300*, 108–112.
[47] J. W. Steed, J. L. Atwood, *Supramol. Chem.* (2nd Ed.), Wiley, New York, 2009, p. 226.
[48] E. Solel, M. Singh, O. Reany, E. Keinan, *Phys. Chem. Chem. Phys.* **2016**, *18*, 13180–13185.
[49] F. Biedermann, W. M. Nau, H.-J. Schneider, *Angew. Chem. Int. Ed.* **2014**, *53*, 11158–11171.
[50] S. Kumar, S. Soni, W. Danowski, C. L. F. van Beek, B. L. Feringa, P. Rudolf, R. C. Chiechi, *J. Am. Chem. Soc.* **2020**, *142*, 15075–15083.
[51] L. Shang, N. Azadfar, F. Stockmar, W. Send, V. Trouillet, M. Bruns, D. Gerthsen, G. U. Nienhaus, *Small* **2011**, *7*, 2614–2620.
[52] L. Srisombat, A. C. Jamison, T. R. Lee, *Colloids and Surfaces A: Physicochem. Eng. Aspects* **2011**, *390*, 1–19.
[53] M. Li, L. Ling, Q. Xia, X. Li, *RSC Adv.* **2021**, *11*, 12757–12770.
[54] W. He, Y. Du, W. Zhou, T. Wang, M. Li, X. Li, *Eur. J. Pharm. Sci.* **2020**, *150*, 105340.
[55] J. Huang, F. Wu, Y. Yu, H. Huang, S. Zhang, J. You, *Org. Biomol. Chem.* **2017**, *15*, 4798–4802.
[56] A. Tschiche, B. N. S. Thota, F. Neumann, A. Schäfer, N. Ma, R. Haag, *Macromol. Biosci.* **2016**, *16*, 811–823.
[57] J. Huang, L. Wang, P. Zhao, F. Xiang, J. Liu, S. Zhang, *ACS Catal.* **2018**, *8*, 5941–5946.

Manuscript received: September 12, 2023
Accepted manuscript online: October 23, 2023
Version of record online: November 23, 2023